Polarized charge transfer spectroscopy of Cu^{2+} in doped one-dimensional $[N(CH_3)_4]CdCl_3$ and $[N(CH_3)_4]CdBr_3$ crystals

1994 J. Phys.: Condens. Matter 6 4527

(http://iopscience.iop.org/0953-8984/6/24/014)

J. Phys.: Condens. Matter 6 (1994) 4527–4540. Printed in the UK

Polarized charge transfer spectroscopy of Cu^{2+} in doped one-dimensional $[N(CH_3)_4]CdCl_3$ and $[N(CH_3)_4]CdBr_3$ crystals

R Valiente, M C Marco de Lucas and F Rodríguez

DCITTYM (Sección Ciencia de Materiales), Facultad de Ciencias, Universidad de Cantabria, 39005-Santander, Spain

Received 17 December 1993

Abstract. This work investigates the polarized charge-transfer (CT) spectra of the Jahn–Teller distorted $CuCl_6^{4-}$ and $CuBr_6^{4-}$ complexes formed in Cu^{2+}-doped $[N(CH_3)_4]CdCl_3$ and $[N(CH_3)_4]CdBr_3$ crystals. The transition energies as well as the dominant polarization of the CT bands along the hexagonal c direction are explained in terms of rhombic D_{2h} distortions. In the bromide complexes, the strong spin–orbit interaction of the Br^- ligands leads to additional bands in the low-temperature spectra. Evidence of vibronic couplings to totally symmetric vibrations is found from analysis of the temperature dependence of the band width.

The influence of Cu^{2+} impurities in the lattice dynamics is studied through the variation undergone by different spectroscopic parameters in the 10–300 K range. Throughout this work, the high sensitivity of CT transitions for detecting the structural phase transitions exhibited by these crystals is demonstrated. In particular, the enhancement of the first-order character of the ferroelectric phase transition in $[N(CH_3)_4]CdBr_3:Cu^{2+}$ at $T_F = 157$ K, which has been associated with the presence of Cu^{2+} impurities is worth noting.

1. Introduction

The hexacoordinate copper(II) complexes CuX_6^{4-} (X ≡ F, Cl or Br) are attractive systems for investigating their optical and magnetic properties due to the variety of structural modifications displayed by these complexes as well as the simple electronic configuration of Cu^{2+} (d^9). An interesting feature of these systems is the strong influence of the geometrical structure upon the optical properties of these complexes which may lead to marked piezochroism or thermochroism when such structural modifications are induced by pressure or temperature [1–4]. Apart from the common elongated D_{4h} symmetry found for CuX_6^{4-}, other geometrical configurations associated either with D_{2h} rhombic distortions or with the compressed D_{4h} symmetry have been found in different copper-doped or pure compounds [5–10]. However, it should be noted that the compressed D_{4h} symmetry for CuX_6^{4-} is very unusual. This geometry has only been identified clearly in fluoride lattices such as the pure crystal $KCuAlF_6$ [11] or Cu^{2+}-doped K_2ZnF_4 [12, 13] and Ba_2ZnF_6 [14]. Although efforts have been made to form compressed complexes in chlorides, they were unsuccessful. An example of this is the recent work carried out in the (3-chloroanilinium)$_8$ $[CuCl_4]Cl_4$ crystal [15]. First x-ray experiments suggested the presence of compressed $CuCl_6^{4-}$ but further investigations employing EPR, polarized optical absorption (OA) spectroscopy, EXAFS and x-ray diffractometry at low tempertures showed that these $CuCl_6^{4-}$ units are actually elongated, forming an antiferrodistortive-type network

0953-8984/94/244527+14$19.50

whose room-temperature x-ray pattern might be interpreted in terms of compressed units [16]. Concerning this, the crystal $(enH_2)MnCl_4:Cu^{2+}$ [17] is a unique system where the presence of compressed $CuCl_6^{4-}$ complexes has been proposed to explain the origin of the red colour exhibited by this copper-doped manganese crystal.

In general, investigations devoted to exploring the optical properties of CuX_6^{4-} complexes have been performed in pure crystals and so the OA spectra are limited to the range of the intraconfigurational ligand-field transitions. The corresponding charge-transfer (CT) spectra remain almost unexplored owing to the higher oscillator strengths of these bands (about 0.1). Although this problem could be overcome by diluting Cu^{2+} in isomorphous crystals, as has been done for the tetrahalides $CuCl_4^{2-}$ and $CuBr_4^{2-}$ of D_{2d} symmetry [9, 18–22], the CT spectra of hexacoordinate complexes are at present very scarce for $CuCl_6^{4-}$ whereas no polarized CT spectrum has been reported for $CuBr_6^{4-}$. The only CT spectrum known for $CuBr_6^{4-}$ was obtained by Kuroda *et al* [23] for cubic LiBr: Cu^{2+} crystals.

This work investigates the CT spectra of CuX_6^{4-} ($X \equiv$ Cl or Br) complexes formed in the one-dimensional $[N(CH_3)]_4CdCl_3$ (TMCC) and $[N(CH_3)]_4CdBr_3$ (TMCB) crystals doped with Cu^{2+} in the 10–300 K temperature range. The reasons for using these crystals as Cu^{2+} hosts is threefold:

(1) They are diamagnetic and transparent in the $X^- \rightarrow Cu^{2+}$ CT region,

(2) These crystals allow easy substitution of Cd^{2+} by Cu^{2+}.

(3) The presence of cationic impurities in the isomorphous TMMC containing manganese has a large influence on the magnetic and luminescence properties [24–27] as well as on the lattice dynamics [28].

The order–disorder $P6_3/m \rightarrow P2_1/a$ phase transition (PT) at $T_c = 126$ K in TMMC, which is associated with the ordering of the tetramethylammonium (TMA) groups, is strongly affected by the doping of TMMC with 2% of Cu^{2+} [28]. A new PT sequence takes place in this Cu^{2+}-doped crystal with transition temperatures of 92, 124 and 134 K. These PTs are probably associated with the prescence of an incommensurate phase stabilized by the Cu^{2+} impurities. It was suggested in [28] that the fairly large interaction between the TMA groups and the Jahn–Teller (JT) distorted $CuCl_6^{4-}$ units could be responsible for such anomalies. In the present case of TMCB: Cu^{2+} and TMCC: Cu^{2+}, special emphasis will be placed on the influence of PTs upon the CT spectra of Cu^{2+} as well as on the role of Cu^{2+} upon the lattice dynamics. In this way, the CT bands of Cu^{2+} complexes are more sensitive than the corresponding ligand-field transitions when used as probes to detect the PT sequence in $NH_4Cl:Cu^{2+}$ [29, 30], $NH_4Br:Cu^{2+}$ [31] and $TMA_2MnCl_4:Cu^{2+}$ [21, 32].

2. Experimental details

Single crystals of TMCC:Cu^{2+} and TMCB:Cu^{2+} were grown by slow evaporation at 39 °C of highly acidified (3 M ClH or BrH) aqueous solutions containing stoichiometric amounts of the corresponding tetramethylammonium and cadmium halides. A 5 mol.% of the copper halide was added to the solutions. The real Cu^{2+} concentrations in both crystals were measured by atomic absorption spectroscopy. Values of 0.075% and 0.070% were obtained for TMCC:Cu^{2+} and TMCB:Cu^{2+} crystals, respectively.

The crystals grown as needles displaying hexagonal prism habits elongated along the c direction. Their crystallographic structure and orientation were checked by x-ray diffraction and polarizing microscopy.

The crystals belong to the hexagonal $P6_3/m$ space group at room temperature. The structure consists of linear chains of face-sharing CdX_6^{4-} octahedra (figure 1). The TMA groups placed between the inorganic chains display an orientational disorder associated with the threefold axis of the molecule pointing along c.

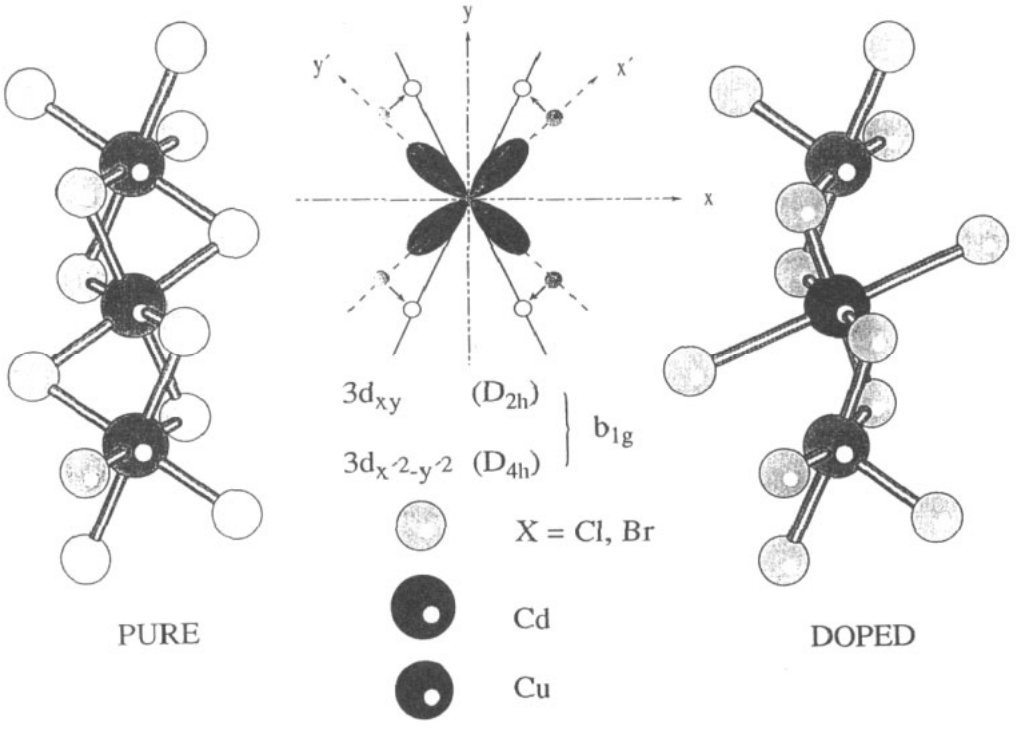

Figure 1. Structure of the inorganic chains in the one-deimensional TMCX (X ≡ Cl or Br) crystals. The local structure around the Cu^{2+} in the doped crystals is shown on the right. Its symmetry is nearly D_{4h} with a small rhombic distortion, D_{2h} (C_2''), associated with the bending of the equatorial Cl^- ligands towards the y axis. Note that the b_{1g} ($d_{x^2-y^2}$) unpaired electron orbital in D_{4h} corresponds to the b_{1g} (d_{xy}) orbital in the D_{2h} symmetry axis.

Spectra were recorded with a Lambda 9 Perkin–Elmer spectrophotometer equipped with Glan Taylor polarizing prisms. Sample path lengths for absorption were about 0.2 mm. The polarized light propagates perpendicular to c with E parallel (π) or perpendicular (σ) to the chain (c direction).

The temperature was stabilized to within 0.05 K in the 9.5–300 K range with a Scientific Instruments 202 closed-circuit cryostat and an APD-K controller.

3. Results

Figure 2 shows the polarized OA spectra of Cu^{2+}-doped TMCC and TMCB crystals at 10 and 297 K. The room-temperature (RT) spectra of both crystals are characterized by the presence of two intense mainly π-polarized bands which are located at 26 700 and 37 400 cm^{-1} in the chloride and at 19 200 and 32 000 cm^{-1} in the bromide. At low temperatures other

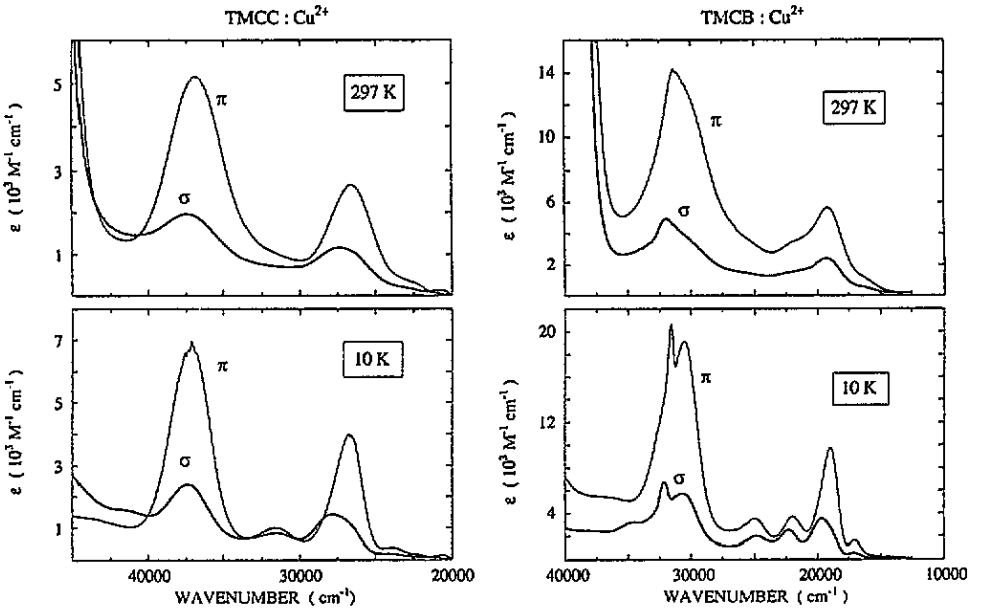

Figure 2. π- and σ-polarized optical absorption spectra of the Cu^{2+}-doped TMCC and TMCB crystals at 297 and 10 K.

bands, masked in the RT spectra, are clearly visible. Although the chloride and bromide spectra are quite similar, the TMCB:Cu^{2+} spectrum shows a more complex structure, with *additional* bands at around 19 000 and 32 000 cm^{-1}.

It is worth pointing out the presence of one mainly σ-polarized band at 27 900 and 19 700 cm^{-1} in TMCC:Cu^{2+} and TMCB:Cu^{2+}, respectively. This band was already observed as a shoulder in the unpolarized RT spectra of $CdCl_2$:Cu^{2+} [33] and also in LiCl:Cu^{2+} [23] together with the 26 700 and 37 400 cm^{-1} bands, although in neither case could information about their polarization be obtained. A similar situation occurs for LiBr:Cu^{2+}. It should also be noted that the peak positions and polarization of these bands for TMCC:Cu^{2+} coincide with those given by Güdel *et al* [17] for TMMC:Cu^{2+}, although the strong overlap between the Cu^{2+} and Mn^{2+} bands in this crystal makes a quantitative analysis of polarization difficult. Table 1 shows the transition energy, polarization and total oscillator strength of these bands for TMCC:Cu^{2+} and TMBC:Cu^{2+}. The oscillator strengths were obtained from the total integrated intensity of each band through the formula

$$f = 3.89 \times 10^{-8} \frac{n}{(n^2+2)^2} \int \epsilon \, dE \tag{1}$$

where ϵ is the molar extinction coefficient, E (cm^{-1}) is the energy and n is the refractive index. Values of $n = 1.5$ and 1.7 were obtained by the Becke method in TMCC:Cu^{2+} and TMCB:Cu^{2+}, respectively. In both cases, the birefringence Δn is less than 10^{-2}.

Figures 3–5 depict the variation in the following spectroscopic parameters with temperature: the total oscillator strength, $f_T = 2f_\sigma + f_\pi$, where f_σ and f_π are the oscillator strengths obtained through equation (1) for the σ and π spectra, respectively; the relative intensity defined by the ratio $f_\pi/(2f_\sigma + f_\pi)$; the transition energy; the band width derived from the first and second band moments. For TMCC:Cu^{2+} this analysis was made in the

Table 1. Assignment of the CT spectra of TMCC:Cu^{2+} and TMCB:Cu^{2+} within D_{4h} and D_{2h} (C_2'') molecular orbital schemes. Transitions from the $^2B_{1g}$ ground state to different CT states are denoted by x, y, z or F depending on whether transitions are polarized along the x, y, z directions or forbidden, respectively. The experimental transition energies and the corresponding oscillator strengths ($f_T = 2f_\sigma + f_\pi$) were obtained from the $T = 10$ K spectra. The dominant polarization is given in parentheses.

Transition assignment		TMMC:Cu^{2+}		TMCB:Cu^{2+}	
D_{4h}	$D_{2h}C_2''$	Energy (eV)	f_T	Energy (eV)	f_T
$^2B_{1g} \rightarrow {}^2A_{2u}$ ($\pi + \sigma$) (F)	$^2B_{1u}$ (F)			16 950 (π)	0.004
$^2B_{1g} \rightarrow {}^2E_u$ ($\pi + \sigma$) (x, y)	$^2B_{2u}$ (y)	26 650 (π)	0.03	19 090 (π)	0.04
	$^2B_{3u}$ (x)			22 310 (π)	0.02
$^2B_{1g} \rightarrow {}^2B_{2u}$ (π) (z)	^2A_u (z)	28 070 (σ)	0.02	19 730 (σ)	0.04
$^2B_{1g} \rightarrow {}^2E_u$ ($\pi + \sigma$) (x, y)	$^2B_{2u}$ (y)	31 600 (π)	0.01	25 080 (π)	0.02
	$^2B_{3u}$ (x)				
$^2B_{1g} \rightarrow {}^2E_u$ ($\sigma + \pi$) (x, y)	$^2B_{2u}$ (y)	37 220 (π)	0.08	31 000 (π)	
	$^2B_{3u}$ (x)			32 100 (π)	0.24
$^2B_{1g} \rightarrow {}^2A_{2u}$ ($\sigma + \pi$) (F)	$^2B_{1u}$ (F)			34 700 (σ)	

highest-energy band, at 37 400 cm^{-1}, while for TMCB:Cu^{2+} the analysis of the band width was made for the peak at 19 090 cm^{-1} in the 10–200 K range since the presence of several components around 32 000 cm^{-1} makes such an analysis in this band difficult.

It is interesting to observe that the variations undergone by these parameters show discontinuities at the PT temperatures. These are particularly important for the bands at 19 090 and 25 080 cm^{-1} in TMCB:Cu^{2+} which experience jumps of about 100 cm^{-1} at $T_c = 157$ K. Furthermore, the linear blue shift followed by all these bands from 297 K to T_c changes below T_c. In the low-temperature phase, the bands experience a continuous red shift which resembles the variation undergone by the order parameter [25, 26]. Similar variations are also found for TMCC:Cu^{2+} although two jumps are detected at $T_{c1} = 118$ K and $T_{c2} = 104$ K.

By contrast, the band widths are not so influenced by the PTs. In both cases, their temperature dependence follows typical hyperbolic cotangent functions $H(T) = H_0[\coth(\hbar\omega/2kT)]^{1/2}$, with vibrational energies $\hbar\omega = 267$ and 157 cm^{-1} for TMCC:Cu^{2+} and TMCB:Cu^{2+}, respectively.

4. Analysis and discussion

4.1. Charge-transfer band assignment

The peak energies and oscillator strengths of the absorption bands in figure 2 are characteristic of ligand X^- to metal Cu^{2+} CT transitions of the formed CuX_6^{4-} (X ≡ Cl or Br) complexes. This statement is also confirmed by the red shift of about 6000 cm^{-1} experienced by these bands when Cl^- is replaced by Br^- ligands, according to the Jørgensen optical electronegativity scale which predicts a shift of the CT transitions given by $\Delta E = 30\,000\ \Delta\chi$, where $\Delta\chi = \chi_{Cl} - \chi_{Br} = 0.2$ is the Cl^--to-Br^- optical electronegativity difference [34]. In addition, the spectra in figure 2 are very similar to those obtained for $CdCl_2$:Cu^{2+} where the $CuCl_6^{4-}$ complexes formed are known to display an elongated D_{4h} symmetry [33]. In fact, the two bands observed in $CdCl_2$:Cu^{2+} at 25 000 and 32 000 cm^{-1} were assigned within a D_{4h} symmetry molecular orbital (MO) framework to electric dipole (ED) transitions coming from the mainly Cl^-e_u ($\pi + \sigma$) and e_u ($\sigma + \pi$) MOs to the mainly

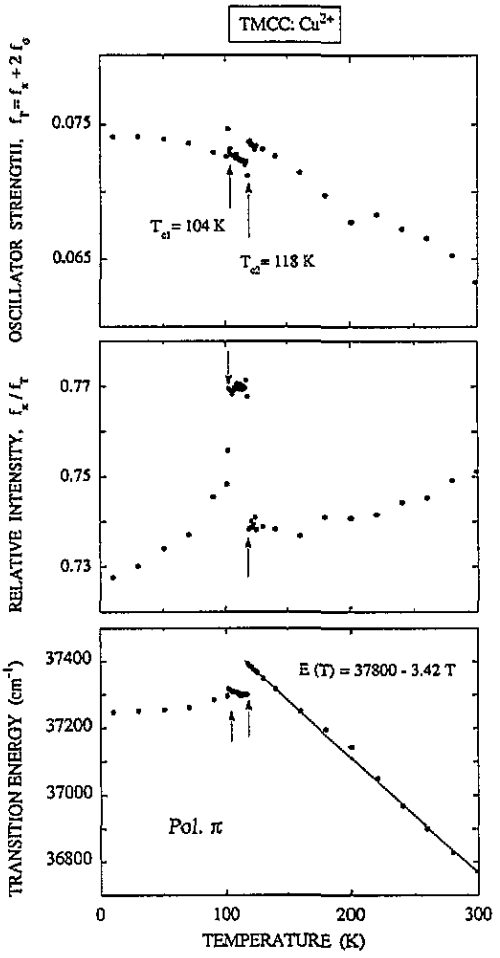

Figure 3. Variation in the total oscillator strength, the relative π intensity and the transition energy of the highest-energy CT band in the 10–300 K range for TMCC:Cu^{2+}.

Cu^{2+} antibonding b_{1g} $(x^2 - y^2)$ MO according to the diagram in figure 6. No evidence of other ED symmetry-allowed CT transitions from the non-bonding b_{2u} (π) and e_u (π) ligand levels was obtained in this system.

The similarity between the CT spectra of the Cu^{2+}-doped TMCC and TMCB crystals and those of $CdCl_2$:Cu^{2+} strongly suggests a D_{4h} symmetry for the present CuX_6^{4-} complexes. Although a strict D_{4h} symmetry is not possible for the JT distorted CuX_6^{4-} complexes given that the symmetry at the substituted Cd^{2+} site is D_{3d}, their real symmetry should not be far from D_{4h} since this is the more common symmetry exhibited by Cu^{2+} placed in nearly octahedral sites. However, this symmetry cannot account for the polarization shown by the bands associated with the $e_u \rightarrow b_{1g}$ CT transitions because we observe that they are mostly polarized along the chain (*c* direction). In fact, if we consider a local D_{4h} symmetry for $CuCl_6^{4-}$ with the long Cu–Cl bond randomly distributed along one of the three *trans* Cl–Cd–Cl directions of the substituted $CdCl_6^{4-}$ octahedron, then the π-to-σ polarization oscillator strength ratio f_π/f_σ, of the $e_u \rightarrow b_{1g}$ bands must be necessarily less than 2, irrespective

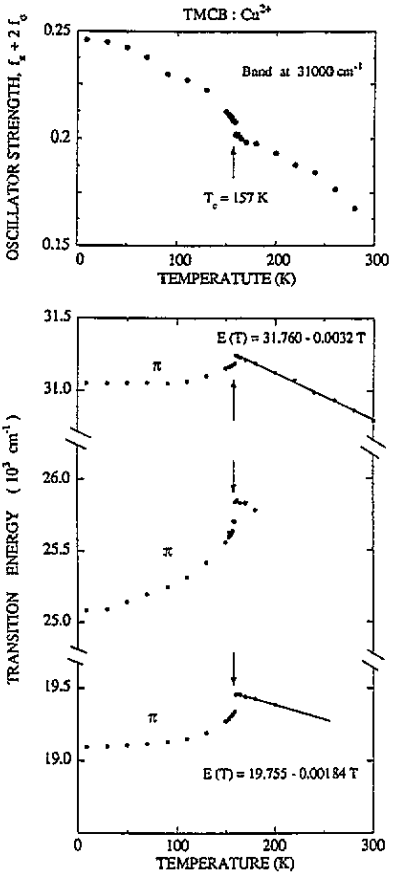

Figure 4. Temperature dependence of the total oscillator strength and the transition energy, derived from the first moment, of several CT bands for TMCB:Cu^{2+}. First-moment analysis for bands at 25 080 and 19 090 cm^{-1} could be made in the 10–200 K range.

of the $CuCl_6^{4-}$ orientation. The π and σ oscillator strengths are $f_\sigma = f_T(1 - \frac{1}{2}\sin^2\alpha)$ and $f_\pi = f_T \sin^2\alpha$, and therefore $I_\pi/I_\sigma = (2\sin^2\alpha)/(1+\cos^2\alpha)$, where α is the angle between the distortion axis (z) of the complex and the c direction. This result indicates that a D_{4h} model cannot explain the experimental value $f_\pi/f_\sigma = 6$ of the mainly π-polarized bands in TMCC:Cu^{2+} and TMCB:Cu^{2+}, even in the most favourable case ($\alpha = 90°$) where $f_\pi/f_\sigma = 2$.

Nevertheless this polarization can be qualitatively explained if we consider a D_{2h} rhombic distortion of the complex. As shown in figure 1, this type of distortion is more favoured than D_{4h} for one-dimensional systems with the TMMC-type structure due to the crystal anisotropy. The actual D_{2h} (C_2'') symmetry is associated with the bending of the equatorial Cu–Cl bonds of the D_{4h} complex towards the c direction without changing the Cu–Cl distances. EXAFS measurements [35, 36] carried out on TMMC:Cu^{2+} confirm this geometry for $CuCl_6^{4-}$ with short Cu–Cl distances $R = 2.29$ Å. The two long Cu–Cl distances, roughly estimated from the EXAFS spectra of [35], are around 3.0 Å.

This geometry of the $CuCl_6^{4-}$ complex contrasts with that found in two-dimensional crystals, such as (cyclam H_4)$CuCl_6$ with $R_{ax} = 3.18$ Å and $R_{eq} = 2.29$ and 2.30 Å [6], or (enH_2)$CuCl_4$ with $R_{ax} = 2.90$ Å and $R_{eq} = 2.31$ and 2.32 Å [7]. These crystals display

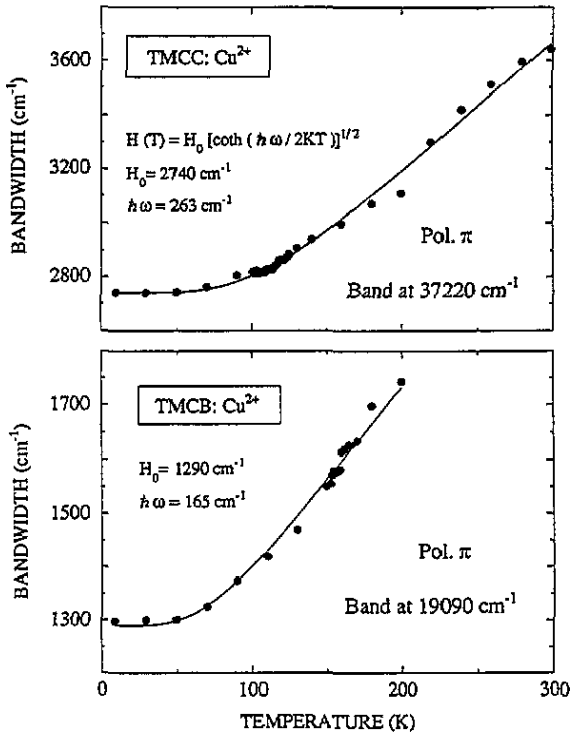

Figure 5. Variation in the band width, derived from the second moment, of the CT bands at 37 220 and 19 090 cm^{-1} in the π spectra of TMCC:Cu^{2+} and TMCB:Cu^{2+}, respectively. Solid lines correspond to the least-square fittings to the equation $H(T) = H_0[\coth(\hbar\omega/2kT)]^{1/2}$.

an antiferrodistortive structure where the nearly D_{4h} $CuCl_6^{4-}$ units exhibit a real rhombic D_{2h} (C_2') symmetry, with three different metal–ligand distances. The existence of these two D_{2h} distortions, C_2' and C_2'', has a large influence on both the EPR and the optical absorption spectra, especially for the CT bands. A salient difference between geometries concerns the electronic ground state. This transforms as a_{1g} or b_{1g} depending on whether the unpaired electron orbital is $d_{x^2-y^2}$ (C_2') or d_{xy} (C_2''), respectively. Note that the x, y coordinate axes are taken along the equatorial Cu–Cl directions for C_2' while they are directed along their diagonals for C_2'' (figure 1). In the former case, the $d_{x^2-y^2}$ orbital mixes with the Cu^{2+} $d_{3z^2-r^2}$ and 4s orbitals, and therefore we can find significant departures in the principal values of the gyromagnetic tensor **g** from those found in elongated D_{4h} complexes. Moreover, this also affects the CT spectra because new ED transitions allowed by symmetry are expected in D_{2h} (C_2') with respect to D_{4h} and D_{2h} (C_2'') (figure 6). EPR and OA measurements in two-dimensional systems would be desirable for clarifying these points.

The D_{2h} (C_2'') scheme in figure 6 accounts well for the OA spectra of the present one-dimensional systems. The four bands observed in the low-temperature spectra of TMCC:Cu^{2+} are assigned according to their polarization and peak energy to the CT transitions indicated in figure 6 and table 1. It is worth pointing out that this is the first system where the presence of one CT band associated with the second e_u MO (D_{4h} notation) is observed. It is also noteworthy the strong dichroism exhibited by the b_{2u} (e_u in D_{4h}) $\rightarrow$ b_{1g} CT bands, which seem to be completely polarized along the y direction of the $CuCl_6^{4-}$ complex (figure 2). However, this behaviour is difficult to reconcile *a priori*, with slight rhombic distortions

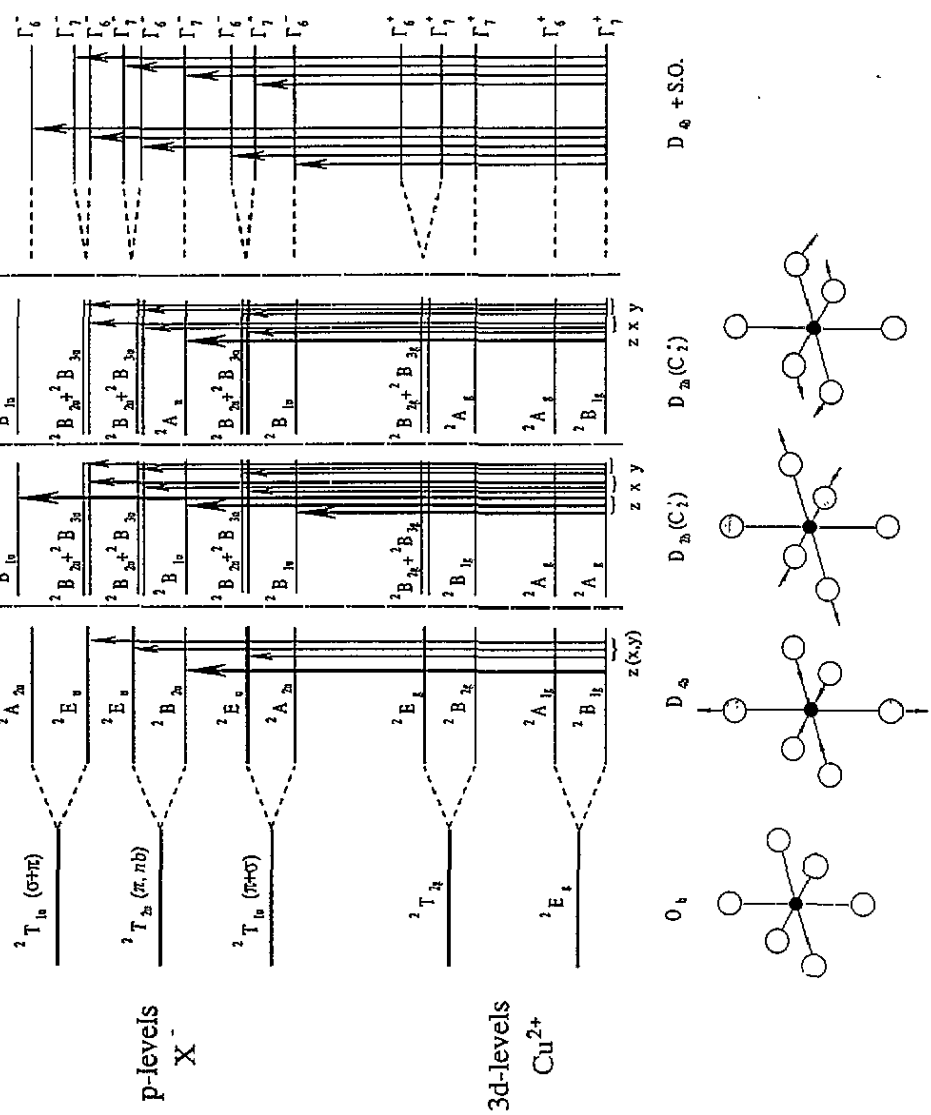

Figure 6. Qualitative energy level diagram for the CuX_6^{4-} complex. The electronic states are denoted by the symmetry label corresponding to the O_h, the elongated D_{4h} and the two possible rhombic distortions D_{2h} (C'_2) and $D_{2h}(C''_2)$. The effect of the spin–orbit interaction of the ligands upon the D_{4h} diagram is shown on the right (Bethe notation is used). The CT states in O_h and D_{4h} were ordered according to the experimental results available for the octahedral $FeCl_6^{3-}$ complex [49] and MS–Xα calculations performed on D_{4h} elongated $CuCl_6^{4-}$ complexes [39]. The arrows indicate the symmetry-allowed electric dipole transitions for each geometry.

since this transition would be x, y polarized in a perfect D_{4h} symmetry. The experimental intensity ratio, $f_\pi/f_\sigma = 6$, clearly suggests that this band uniquely corresponds to the y-polarized $b_{2u} \rightarrow a_{1g}$ transition (D_{2h} (C_2'')). With this assumption, the experimental value is close to that expected if the equatorial plane of the $CuCl_6^{4-}$ complex coincides with that of the $CdCl_6^{4-}$ octahedra in the perfect lattice: $f_\pi/f_\sigma = 2\cot^2\beta$, where $\beta = 31.2°$ is the angle that the equatorial plane makes with c [32]. Analogously, this model allows us to confirm the assignment of the CT band at 28 070 cm^{-1} to the a_u (b_{2u} in D_{4h}) $\rightarrow$ b_{1g} transition, which must be polarized along the z direction of the complex. In fact, the experimental π-to-σ intensity ratio $f_\pi/f_\sigma = 0.8$ for that band obtained by fitting the OA spectra in the 20 000–30 000 cm^{-1} range to the sum of two Gaussians, is similar to the expected value $f_\pi/f_\sigma = 2\cot^2(90° - \beta)$, for $\beta = 31.2°$. This result, together with the structural data obtained from EXAFS for TMMC:Cu^{2+}, justifies the geometrical structure proposed for $CuCl_6^{4-}$ and sketched in figure 1. The values of the interatomic distances in the complex (2.29 and 3.0 Å for Cu–Cl bonds, and 2.64 Å for the Cd–Cl distances) and the angle $\beta = 31.2°$ lead to Cl–Cl distances within the equatorial plane of 3.10 Å and 3.24 Å, along the x and y directions, respectively. This figure explains, qualitatively the oscillator strength enhancement observed along the c direction taking into account that the oscillator strength of the b_{2u} and $b_{3u} \rightarrow b_{1g}$ CT transitions are mainly governed by the p_σ orbitals of the Cl^- ligands. The modules of the non-zero matrix elements $\langle b_{3u}|x|b_{1g}\rangle$ and $\langle b_{2u}|y|b_{1g}\rangle$, which are equal in D_{4h}, must be different in D_{2h} (C_2''). An increase in $|\langle b_{2u}|y|b_{1g}\rangle|^2$ and a decrease in $|\langle b_{3u}|x|b_{1g}\rangle|^2$ are expected for the C_2'' distortion of figure 1 since the Cl–Cu–Cl bending along the y direction increases the ligand charge density in this direction and decreases it along x. This simple picture explains the observed polarization although precise calculations of those matrix elements for several D_{2h} distortions would be useful in order to establish structural correlations.

4.2. Influence of the spin-orbit interaction in the CT spectra

Apart from the peak energies, the similarity between the RT spectra of the isomorphous TMCC:Cu^{2+} and TMCB:Cu^{2+} makes the CT band assignment easy. The bands at 19 000 cm^{-1} and 31 000 cm^{-1} correspond to the two $e_u(\pi+\sigma)$ and $e_u(\sigma+\pi) \rightarrow b_{1g}$ CT transitions within a D_{4h} MO framework. However, an important difference between these two crystals is the presence of additional CT bands in the low-temperature spectra of TMBC:Cu^{2+} (figure 2). This feature, which was also observed in the tetracoordinated CuX_4^{2-} (X ≡ Cl or Br) complexes of D_{2d} symmetry [20, 22], is explained in terms of the larger spin–orbit interaction of the Br^- ligands ($\xi_{4p} = 2480$ cm^{-1} and $\xi_{3p}(Cl)/\xi_{4p}(Br) \simeq 0.25$) [37]. For $CuBr_6^{4-}$, this interaction is of the same order as the D_{2h} ligand field, and therefore the spin–orbit splitting of the ligand states can be detected spectroscopically. The effect of the spin–orbit interaction on the CT spectra of $CuBr_6^{4-}$ is twofold: firstly the tetragonal $^2E_u + {}^2B_{2u}$ and $^2E_u + {}^2A_{2u}$ states coming from the parent $^2T_{2u}$ and $^2T_{1u}$ octahedral states split several thousand wavenumbers into $2\Gamma_6^- + \Gamma_7^-$ and $\Gamma_6^- + 2\Gamma_7^-$ (double-group irreducible representations in Bethe notation), respectively; secondly CT transitions coming from the $^2B_{1g}(\Gamma_7^+)$ ground state are ED allowed to states transforming as Γ_7^- (x, y, z polarized) or Γ_6^- (x, y polarized). This means that transitions from the ground state to every odd-parity CT state are allowed by symmetry.

Although the present arguments indicate that the CT transitions can be polarized along x, y or z, most bands as in $CuCl_6^{4-}$ are mainly polarized along c. This behaviour can be understood using the same scheme followed for $CuCl_6^{4-}$ where the mainly π-polarized bands were associated with the $^2B_{1g} \rightarrow {}^2B_{2u}$ transition. According to this, the presence of additional bands mainly polarized along c (table 1) is due to the mixing with the $^2B_{2u}$ state by the spin–orbit interaction.

The peak energies, oscillator strengths and assignments of the $CuBr_6^{4-}$ CT bands are listed in table 1. Two facts must be emphasized: firstly the largest splitting is observed for the first CT band associated with the $^2T_{1u}(\pi+\sigma)$ octahedral state (this result was also found for $CuBr_4^{2-}$ complexes [22]); secondly the oscillator strengths for $CuBr_6^{4-}$ are three times those for the $CuCl_6^{4-}$ (this demonstrates the higher metal–ligand overlap expected for the more covalent $CuBr_6^{4-}$ complex).

4.3. Temperature dependences: influence of phase transitions

The variations in the different spectroscopic parameters, shown in figures 3 and 4 for TMCC:Cu^{2+} and TMCB:Cu^{2+}, reveal anomalies at the PT temperatures. The less sensitive of these parameters to the phase transformation is the band width (figure 5). Its variation reflects the coupling of the CT states to totally symmetric vibrations which are associated with stretching modes of the equatorial ligands of a_g symmetry. This is clearly evidenced through the vibrational energies derived by fitting the temperature dependence of the band width to the equation $H(T) = H_0[\coth(\hbar\omega/2kT)]^{1/2}$. The values $\hbar\omega = 263$ cm^{-1} for $CuCl_6^{4-}$ and 165 cm^{-1} for $CuBr_6^{4-}$ are similar to those found by Raman spectroscopy for the a_{1g} mode of the equatorial ligands in the square planar (creatinium)$_2CuCl_4$ (290 cm^{-1}) [38], and in the $CuCl_6^{4-}$-elongated (cyclam H_4)$CuCl_6$ (262 cm^{-1}) and (metH)$_2$ $CuCl_4$ (275 cm^{-1}) [6]. The fact that these frequencies are somewhat larger than the corresponding $CdCl_6$ frequencies of the pure crystal confirms the geometrical structure proposed for these $CuCl_6^{4-}$ complexes. The same a_{1g} mode is assumed for $CuBr_6^{4-}$ since its frequency essentially corresponds to $(m_{Cl}/m_{Br})^{1/2}$ times the $CuCl_6^{4-}$ frequency.

Interestingly, the relative π intensity f_π/f_T, of the $^2B_{1g} \rightarrow {}^2B_{2u}$ transition at 37 000 cm^{-1} in TMCC:Cu^{2+} gives directly $\cos^2\beta$, assuming that this band is completely polarized along the local y axis of the complex. Therefore, this parameter allows us to follow the orientation of the $CuCl_6^{4-}$ complex with temperature. Note that β remains almost constant in the $P6_3/m$ phase (300–118 K); it experiences an abrupt increase $\Delta\beta = +2°$ at the $P6_3/m \rightarrow P2_1/m$ PT temperature $T_{c1} = 118$ K and decreases by $\Delta\beta = -1°$ at the $P2_1/m \rightarrow P2_1/b$ PT temperature $T_{c2} = 104$ K. Below this temperature, β continuously decreases about 2° from 104 to 10 K. This result must be compared with the variation undergone by the corresponding peak energy. This band experiences a linear blue shift of 620 cm^{-1} between 300 and 118 K according to the variation expected for a decrease in the equatorial Cu–Cl distances by thermal contraction [39]. The red-shift jump of 100 cm^{-1} observed at T_{c1} points out a local expansion of the complex associated with this PT. The $P2_1/m \rightarrow P2_1/b$ PT is evidenced by the change in slope at T_{c2}. Below this temperature there is a continuous red shift down to 10 K, probably due to an anomalous local thermal expansion around Cu^{2+}. It should be noted that anomalous relaxations around impurities have also been detected in the $P\bar{4}3m$ phase of Cu^{2+}-doped NH_4Cl below $T_c = 242.5$ K, by OA and Raman spectroscopy [40]. Nevertheless, such a local expansion for TMCC:Cu^{2+} could be actually reflecting the lattice dynamics, in view of the structural data reported by Couzi *et al* [41] on pure TMCC crystals, where the nearest Cd–Cd distance along the chain increases from 3.33 Å at 100 K to 3.35 Å at 45 K.

The results for TMCB:Cu^{2+} are similar to those for TMCC:Cu^{2+} although an analysis of the parameter f_π/f_T for the band at around 32 000 cm^{-1} is not easy owing to the presence of σ-polarized components.

The variation in the total oscillator strength as well as of the peak energies (figure 4) reveals also anomalies at the $P6_3/m \rightarrow P6_1$ ferroelectric PT temperature $T_F = 157$ K. The peak energies of the three selected bands show similar temperature dependences which

resemble the variation followed by the order parameter given by the spontaneous polarization [42, 43]. It is interesting to observe the higher sensitivity of the CT band at 25 500 cm^{-1} for detecting the ferroelectric PT. Future calculations of the transition energies as a function of the metal–ligand distances and the complex geometry may clarify this distinct behaviour.

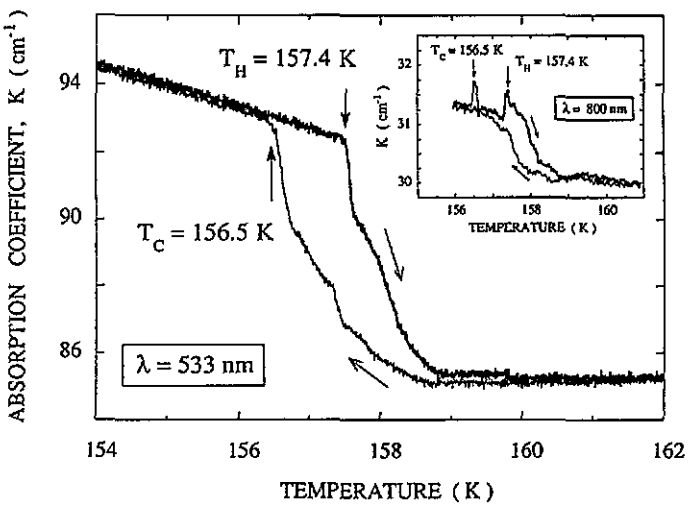

Figure 7. Temperature dependence of the absorption coefficient around the ferroelectric phase transition of TMCB:Cu^{2+}. The selected wavelengths provide the maximum variation in the CT spectra (533 nm) and the absorption background (800 nm). The peaks observed in the cooling (T_C = 156.5 K) and heating (T_H = 157.4 K) runs for λ = 800 nm reveal critical scattering at the PT temperature. These peaks are not detected for λ = 533 nm because of the local character of the Cu^{2+} probe.

In order to explore the role of the Cu^{2+} impurities on the PT dynamics, we have made precise measurements of the PT temperature and the thermal hysteresis in TMCB:Cu^{2+}. Figure 7 depicts the variation in the crystal absorption coefficient at 18 870 cm^{-1} (530 nm) and 12 500 cm^{-1} (800 nm) around T_F. The curves were obtained making continuous heating–cooling runs at rates of 0.15 K min^{-1}. The selected wavelengths allow us to follow the PT dynamics in the complex and in the crystal independently. This procedure was employed with success for detecting the PT sequence in TMA_2MnCl_4:Cu^{2+} [32, 44] and in the mixed $NH_4Br_{1-x}Cl_x$:Cu^{2+} crystals [45, 46]. The results clearly show that the $CuBr_6^{4-}$ complex follows the crystal dynamics. However, the measured thermal hysteresis ΔT = 0.9 K is somewhat larger than the value of 0.2 K obtained by Vanek *et al* [47] for pure crystals through dielectric techniques. This increase in the first-order character of the ferroelectric PT is attributed to the presence of Cu^{2+}, in line with the discussion in [28]. The interactions between the CdX_6^{4-} octahedra and the TMA molecules governing the PT may be largely increased by the presence of JT elongated CuX_6^{4-} complexes and thus they affect the TMA ordering.

Finally, it must also be pointed out that no evidence of the PT at T = 183 K reported by Kahrizi *et al* [48] by thermal dilatometry has been found through the present spectroscopic tools. This is in agreement with the dielectric measurements carried out by Gesi [42]. who detected only one PT at T_F = 156 K.

Acknowledgments

We thank Professor Verdaguer and Dr Dupas for helpful discussions and for providing us with useful information about EXAFS measurements on TMMC:Cu^{2+}. This work has been supported by the CICYT under project number PB 92-0505 and by Caja Cantabria.

References

[1] Willet R D, Ferraro J R and Choca M 1974 *Inorg. Chem.* **13** 2919
[2] Harlow R L, Wells W J, Watt G W and Simonsen S H 1974 *Inorg. Chem.* **13** 2106
[3] Bray K L and Drickramer H G 1990 *J. Phys. Chem.* **94** 2159
[4] Scott B and Willet R D 1991 *J. Am. Chem. Soc.* **113** 5223
[5] Smith D W 1976 *Coord. Chem. Rev.* **21** 93
[6] Khomskii D I and Kugel I 1973 *Solid State Commun.* **13** 763
[7] Tichy K, Benes J, Hälg W and Arend H 1978 *Acta Cryst.* **B34** 2970
[8] McDonald R G and Hitchman M A 1989 *Inorg. Chem.* **28** 3996
[9] Desjardins S R, Penfield K W, Cohen S L, Musselman R L and Solomon E I 1983 *J. Am. Chem. Soc.* **105** 4590
[10] Oelkrug D 1978 *Structure and Bonding* **9** 1
[11] Finnie K, Dubicki L, Krauz E R and Riley M J 1990 *Inorg. Chem.* **29** 3908
[12] Riley M J, Hitchman M A and Reinen D 1986 *Chem. Phys.* **102** 11
[13] Riley M J, Dubicki L, Moran G, Krausz E R and Yamada I 1990 *Chem. Phys.* **145** 363
[14] Reinen D, Steffen G, Hitchman M A, Stratemeier H, Dubicki L, Krausz E R, Riley M J, Mathies H E, Recker K and Wallrafen F 1991 *Chem. Phys.* **155** 117
[15] Tucker D, White P S, Trojan K L, Kirk M L and Hatfield W E 1991 *Inorg. Chem.* **30** 823
[16] Hitchman M A 1994 *Comm. Inorg. Chem.* **15** 197 and references quoted therein
[17] Schmid U, Güdel H U and Willet R D 1982 *Inorg. Chem.* **21** 2977
[18] Ferguson J 1964 *J. Chem. Phys.* **40** 3406
[19] Sharnoff M and Reimann C W 1967 *J. Chem. Phys.* **46** 2634
[20] Bird B D and Day P 1968 *J. Chem. Phys.* **49** 392
[21] Marco de Lucas M C, Rodríguez F and Aramburu J A 1991 *J. Phys.: Condens. Matter* **3** 8945
[22] Marco de Lucas M C and Rodríguez F 1993 *J. Phys.: Condens. Matter* **5** 2625
[23] Hirako S and Onaka R 1982 *J. Phys. Soc. Japan* **51** 1255
[24] Yamamoto H, McClure D S, Marzzacco and Waldman M 1977 *Chem. Phys.* **22** 79
[25] Auerbach R A and McPherson G L 1986 *Phys. Rev.* B **33** 6815
[26] Knochenmuss R and Güdel H U 1987 *J. Chem. Phys.* **86** 1104
[27] Rodríguez W J, Auerbach R A and McPherson G L 1986 *J. Chem. Phys.* **85** 6442
[28] Levola T, Lahio R 1986 *J. Phys. C: Solid State Phys.* **19** 6931
[29] Breñosa A G, Moreno M and Rodríguez F 1987 *Solid State Commun.* **63** 543
[30] Rodríguez F, Breñosa A G, Aramburu J A, Moreno M and Calleja J M 1987 *J. Phys. C: Solid State Phys.* **20** L641
[31] Breñosa A G, Rodríguez F and Moreno M 1988 *J. Phys. C: Solid State Phys.* **21** L623
[32] Marco de Lucas M C and Rodríguez F 1992 *Ferroelectrics* **125** 159
[33] Kan'no K, Naoe S, Mukai S and Nakai Y 1973 *Solid State Commun.* **13** 1325
[34] Jørgensen C K 1970 *Prog. Inorg. Chem.* **12** 101
[35] Clement S, Dupas C and Verdaguer M 1985 *Proc. Conf.: Progress in X-ray Studies by Synchrotron Radiation* **3** 10
[36] Michalowicz A, Verdaguer M, Mathey Y and Clement R 1988 *Topics in Current Chemistry* vol 145 (Berlin: Springer) p 107
[37] Presser N, Ratner M A and Sundheim B R 1978 *Chem. Phys.* **31** 281
[38] McDonald R G and Hitchman M A 1986 *Inorg. Chem.* **25** 3273
[39] Aramburu J A and Moreno M 1989 *J. Chem. Phys.* **86** 871
[40] Breñosa A G, Moreno M, Rodríguez F and Couzi M 1991 *Phys. Rev.* B **44** 9859
[41] Braud M N, Couzi M, Canh N B, Courseille C, Gallois B, Hauw C and Meresse A 1990 *J. Phys.: Condens. Matter* **2** 8209
[42] Gesi K 1990 *J. Phys. Soc. Japan* **59** 432

[43] Aguirre-Zamalloa G, Couzi M, Canh M B and Gallois B 1990 *J. Physique* **51** 2135
[44] Marco de Lucas M C, Rodríguez F and Moreno M 1990 *Ferroelectrics* **109** 21
[45] Breñosa A G, Rodríguez F and Moreno M 1990 *Ferroelectrics* **106** 187
[46] Breñosa A G, Rodríguez F and Moreno M 1993 *Solid State Commun.* **85** 135
[47] Vanek P, Havrankova V M, Smutny F S and Brezina B 1990 *Ferroelectrics* **109** 51
[48] Kahrizi M and Steinitz M U 1989 *Solid State Commun.* **70** 599
[49] Neuenschwander K, Güdel H U, Collingwood J C and Schatz P N 1983 *Inorg. Chem.* **22** 1712